TECHNISCHE MECHANIK, 32, 2-5, (2012), 146 – 154
submitted: October 17, 2011

Modeling Silicon under Contact Loading Conditions: Aspects of Non-Associated Flow

M. Budnitzki, M. Kuna

Technologically relevant abrasive machining techniques (lapping, sawing, grinding) for silicon (Si) are based on (sub-)surface crack formation triggered by contact events. Therefore, the understanding of the inelastic deformation of Si under contact (indenter-)loading is essential to improve machining results. It has been long established that Si undergoes a series of stress driven phase transitions under compression. During subsequent pressure release part of the transformation strain is recovered. The present paper highlights the importance of the direction of inelastic flow for modeling (partially) reversible stress induced phase transitions in materials such as silicon. A phenomenological constitutive model for Si under contact loading, which captures both the $cd{-}Si \rightarrow \beta{-}Si$ transition upon compression and the $\beta{-}Si \rightarrow a{-}Si$ transition upon rapid decompression has been recently presented (Budnitzki and Kuna, 2012). It is shown that indentation experiments are particularly well suited to determine material parameters for this model. Further, material parameters obtained from indentation experiments with Berkovich indenter are confirmed to be valid for the numerical simulation of Knoop indentation, thus verifying a certain predictive capability of the constitutive model.

1 Introduction

The material removal mechanism of technologically relevant abrasive machining techniques for silicon (Si), such as lapping, sawing and grinding, is chipping due to (sub-)surface crack formation triggered by contact events. The evolution of the lateral crack system responsible for the formation of chips is governed by residual stresses (Lawn, 1993, Ch. 8.1.3). Therefore, the understanding of the inelastic deformation of Si under contact (indenter-)loading is essential to improving machining results.

It is known that Si undergoes a series of stress driven phase transitions upon compression and subsequent pressure release. As many as 12 distinct crystalline or amorphous phases of Si have been experimentally observed at various stress levels (Domnich and Gogotsi, 2002; Hu et al., 1986; Mcmahon and Nelmes, 1993; Mcmahon et al., 1994). Gerk and Tabor (1978) suggested that the cd-Si $\rightarrow$ β-Si transition is the governing deformation mechanism for silicon under indenter loading. In this semiconductor to metal transition, diamond-cubic Si (cd-Si, space group $Fd3m$) transforms to the β-tin structure (β-Si, space group $I4_1/amd$), leading to $\sim 20\%$ densification (Hu et al., 1986). This will be referred to as forward transformation. Upon release of pressure the initial diamond-cubic structure is not restored, but replaced by a mixture of different crystalline phases for slow, and amorphous silicon (a-Si) for fast unloading respectively. This will be referred to as reverse transformation. It is therefore clear that isochoric plasticity models employed by some authors (Zhang and Mahdi, 1996; Yoshino et al., 2001; Bhagavat and Kao, 2007; Wang et al., 2007) are but a rough approximation of the inelastic behavior of Si, leading to an incorrect prediction of the residual stresses after unloading, which are the driving force for lateral crack propagation.

Several constitutive models for silicon that consider volume changes during phase transformation exist in literature. The group of Kiriyama et al. (2009) used a multilinear "elastic" model with tangent moduli depending on the direction of loading in order to fit the force displacement ($F-U$) hysteresis obtained in nanoindentation experiments. However, thermomechanical consistency of this approach is questionable. In addition, such a model can neither capture the effect of multiaxiality on the phase transition nor the independent evolution of volumetric and deviatoric inelastic strains. The incremental model introduced by Vodenitcharova and Zhang (2003, 2004) employed ellipsoidal yield/transformation surfaces with an associated flow rule to account for dilatancy effects. However, they did not incorporate the continuous β-Si $\rightarrow$ a-Si phase transition upon decompression, but rather included discrete jumps in the inelastic volumetric strain in order to account for pop-in/out events. Due to the limitations of this approach, the experimental $F-U$ curve could only be fitted by choosing unrealistic values for the elastic

constants ($E = 80$ GPa, $\nu = 0.17$). The commonly known polycrystalline averages for Si are $E = 163$ GPa, $\nu = 0.23$ (Cook, 2006). Further, the model overestimates the size of the transformation zone (Vodenitcharova and Zhang, 2004). In none of the above publications it was attempted to verify the obtained material parameters by simulating an independent load case, which the constitutive models were not explicitly fitted to.

To overcome the deficiencies mentioned above, a novel thermomechanical constitutive model for silicon that captures the cd-Si $\rightarrow$ β-Si transition during contact loading (forward transformation) as well as the β-Si $\rightarrow$ a-Si transition during rapid unloading (reverse transformation) was introduced by Budnitzki and Kuna (2012). Its main constitutive equations are summarized in Sections 4 and 5.

The aim of the present paper is twofold: first, to discuss the mostly neglected aspect of reverse phase transformation (β-Si $\rightarrow$ a-Si) during unloading with particular emphasis on the importance of the direction of inelastic flow (see Sec. 3), and second, to propose a strategy for the successful identification of material parameters for the constitutive model of Budnitzki and Kuna (2012). Subsequently, we show that the material parameters identified from BERKOVICH indentation experiments have general validity (see Sec. 7).

2 Thermomechanics Framework

The isothermal portion of the materials' behavior is fully defined by specifying a thermodynamic state function $\mathscr{E}(\boldsymbol{\sigma}, \boldsymbol{\alpha})$ and a dissipation function $\mathscr{D}(\boldsymbol{\sigma}, \dot{\boldsymbol{\alpha}}, \boldsymbol{\alpha})$, where $\boldsymbol{\sigma}$ denotes the stress and $\boldsymbol{\alpha}$ a set of internal variables. The corresponding generalized stresses (or thermodynamic forces) are defined as $\boldsymbol{\chi} := \partial \mathscr{E}(\boldsymbol{\sigma}, \boldsymbol{\alpha}) / \partial \boldsymbol{\alpha}$. If non-associated flow is considered, $\mathscr{D}$ has to be a function of $\boldsymbol{\sigma}$ (Ziegler and Wehrli, 1987). However, in the following argumentation $\boldsymbol{\sigma}$ is a passive variable and therefore dropped for brevity.

For rate-independent materials, $\mathscr{D}$ is first-order homogeneous in $\dot{\boldsymbol{\alpha}}$. Further, assuming maximal rate of entropy production, which is also known as principle of maximal rate of dissipation and equivalent to Ziegler's orthogonality principle (Ziegler and Wehrli, 1987; Ziegler, 1983), it can be shown (Han and Reddy, 1999) that the generalized stresses are given by $\boldsymbol{\chi} \equiv \partial \mathscr{D}(\dot{\boldsymbol{\alpha}}, \boldsymbol{\alpha}) / \partial \dot{\boldsymbol{\alpha}}$ and are constrained to a closed convex set $K = \{\boldsymbol{\chi} : \Phi(\boldsymbol{\chi}, \boldsymbol{\alpha}) \leq 0\}$ called the elastic region. No dissipation occurs when $\boldsymbol{\chi}$ is in the interior of K. The Legendre-Fenchel transform $\mathscr{D}^*(\boldsymbol{\chi}, \boldsymbol{\alpha}) = \sup_{\dot{\boldsymbol{\alpha}}}[\boldsymbol{\chi}\dot{\boldsymbol{\alpha}} - \mathscr{D}(\dot{\boldsymbol{\alpha}}, \boldsymbol{\alpha})]$ of the dissipation function $\mathscr{D}(\dot{\boldsymbol{\alpha}}, \boldsymbol{\alpha})$ is the indicator function of K, i.e. $\mathscr{D}^*(\boldsymbol{\chi}, \boldsymbol{\alpha}) \equiv I_K$. From the properties of the Legendre-Fenchel transform immediately follows

$$\dot{\boldsymbol{\alpha}} \in \partial_{\boldsymbol{\chi}} \mathscr{D}^*(\boldsymbol{\chi}, \boldsymbol{\alpha}) \equiv \partial I_K =: N_K(\boldsymbol{\chi}, \boldsymbol{\alpha}), \tag{1}$$

where $\partial_{\boldsymbol{\chi}}(\cdot)$ is called the subdifferential with respect to $\boldsymbol{\chi}$ and $N_K(\boldsymbol{\chi}, \boldsymbol{\alpha})$ denotes the cone of outward normals of K. For any regular point on the limit surface $\Phi(\boldsymbol{\chi}, \boldsymbol{\alpha}) = 0$ the cone $N_K(\boldsymbol{\chi}, \boldsymbol{\alpha})$ reduces to the unique outward normal, i.e.

$$\dot{\boldsymbol{\alpha}} = \dot{\lambda} \frac{\partial \Phi(\boldsymbol{\chi}, \boldsymbol{\alpha})}{\partial \boldsymbol{\chi}} \tag{2}$$

for some $\dot{\lambda} \geqslant 0$ [see e.g. Han and Reddy (1999)]. The relationship with the limit surface in true stress space $F(\boldsymbol{\sigma}, \boldsymbol{\alpha})$ is established by $\boldsymbol{\chi} = \partial \mathscr{E}(\boldsymbol{\sigma}, \boldsymbol{\alpha}) / \partial \boldsymbol{\alpha}$, i.e

$$F(\boldsymbol{\sigma}, \boldsymbol{\alpha}) = \Phi\left(\frac{\partial \mathscr{E}(\boldsymbol{\sigma}, \boldsymbol{\alpha})}{\partial \boldsymbol{\alpha}}, \boldsymbol{\alpha}\right) = 0. \tag{3}$$

The internal state variables are commonly chosen as $\boldsymbol{\alpha} = \{\boldsymbol{\varepsilon}^{\mathrm{tr}}, \xi\}$, where $\boldsymbol{\varepsilon}^{\mathrm{tr}}$ is the transformation strain tensor. The relationship between $\dot{\xi}$ and $\dot{\lambda}$ is immediately established by (2). Hence, the phase content of the dense phase ξ plays the role of a consistency parameter, such that the classical Kuhn-Tucker conditions are

$$\dot{\xi} \geq 0, \quad \Phi_f \leq 0, \quad \dot{\xi}\Phi_f = 0; \tag{4}$$

$$\dot{\xi} \leq 0, \quad \Phi_r \leq 0, \quad \dot{\xi}\Phi_r = 0. \tag{5}$$

Here $\Phi_f(\boldsymbol{\chi}, \boldsymbol{\alpha})$ and $\Phi_r(\boldsymbol{\chi}, \boldsymbol{\alpha})$ are the limit surfaces for forward and reverse transformation respectively. The model is completed by requiring

$$0 \leq \xi \leq \hat{\xi}, \tag{6}$$

where $\hat{\xi}$ is the maximal achievable phase content. For materials, such as Si, exhibiting a change in density during the phase transformation, the phase content is directly proportional to the volumetric transformation strain $\nu^{\mathrm{tr}} :=$

$-\operatorname{tr}(\boldsymbol{\varepsilon}^{\mathrm{tr}})$, such that $\xi = \nu^{\mathrm{tr}}/\hat{\nu}^{\mathrm{tr}}$, where $\hat{\nu}^{\mathrm{tr}}$ is the maximal achievable volumetric transformation strain. Finally, the introduction of the deviatoric transformation strain $\boldsymbol{\gamma}^{\mathrm{tr}} := \boldsymbol{\varepsilon}^{\mathrm{tr}} + \frac{1}{3}\nu^{\mathrm{tr}}\mathbf{1}$ allows to conveniently reformulate the choice of internal variables to $\boldsymbol{\alpha} = \{\boldsymbol{\gamma}^{\mathrm{tr}}, \nu^{\mathrm{tr}}\}$. The associated thermodynamic forces are $\boldsymbol{\chi} = \{\boldsymbol{\chi}', \chi_{\mathrm{p}}\}$ with $\boldsymbol{\chi}'$ being the deviatoric and χ_{p} the volumetric parts, respectively.

3 On the Importance of the Direction of Flow

Although the diamond-cubic structure is not restored after unloading a sharp contact in Si, part of the transformation strain is recovered during the β-Si → a-Si transition. The effect of the direction of inelastic flow on the strain recovery during unloading is investigated in this section. In the following, $\|\boldsymbol{A}\| := \sqrt{\boldsymbol{A} : \boldsymbol{A}}$ denotes the norm of a second order tensor $\boldsymbol{A}$ and $\boldsymbol{A}' := \boldsymbol{A} - \frac{1}{3}\operatorname{tr}(\boldsymbol{A})$ denotes its deviator. Further, the notation $A_{\mathrm{q}} := \sqrt{\frac{2}{3}}\|\boldsymbol{A}'\|$ is used.

3.1 An Illustrative Example

As the precise shape of the limit functions only plays a minor role in this discussion, the well-understood Drucker-Prager limit function is used for illustration, i.e. $F_{\mu}(\boldsymbol{\sigma}, \boldsymbol{\alpha}) = \sigma_{\mathrm{q}} + 3\kappa p - Y_{\mu}(\xi)$ with $\mu \in \{f, r\}$, where $\kappa \geqslant 0$ is a constant, p denotes the hydrostatic pressure and $Y_{\mu}(\xi)$ plays the role of a limit stress. This choice already has the main features of the limit functions introduced in Sec. 5, particularly their pressure dependence. For simplicity, the associated case is discussed here and rate equation (2) takes the form

$$\dot{\boldsymbol{\varepsilon}}^{\mathrm{tr}} = \dot{\xi}\frac{\partial F_{\mu}(\boldsymbol{\sigma}, \boldsymbol{\alpha})}{\partial \boldsymbol{\sigma}} = \dot{\xi}\left(\frac{3}{2}\frac{\boldsymbol{\sigma}'}{\sigma_{\mathrm{q}}} - \kappa\mathbf{1}\right) =: \dot{\xi}\boldsymbol{N}(\boldsymbol{\sigma}) \ . \tag{7}$$

Consider a closed, tripartite loading path that connects a series of stress states $\mathscr{S}_0 \xrightarrow{\pi_1} \mathscr{S}_1 \xrightarrow{\pi_2} \mathscr{S}_2 \xrightarrow{\pi_3} \mathscr{S}_0$:

- (π_1) the load is increased proportionally until the limit surface is reached and further until *completion* of the semiconductor to metal (cd-Si → β-Si) transition
- (π_2) the stress state is shifted to another point *on* the limit surface; as the phase transformation has already been completed, this process is purely *elastic*
- (π_3) the load is decreased proportionally, until the initial stress state is reached

This is schematically illustrated in Fig. 1. It should be emphasized that step (π_2) is indeed elastic. Since no 'reorientation' is incorporated into Eq. (7), all state variables are frozen after completion of the forward transformation as a consequence of inequality (6). During loading, the existence of this additional constraint is the essential feature distinguishing phase transformation from a conventional plasticity formulation. For the sake of completeness, it is worth noting that an elastic relocation to a different point on the limit surface is possible even

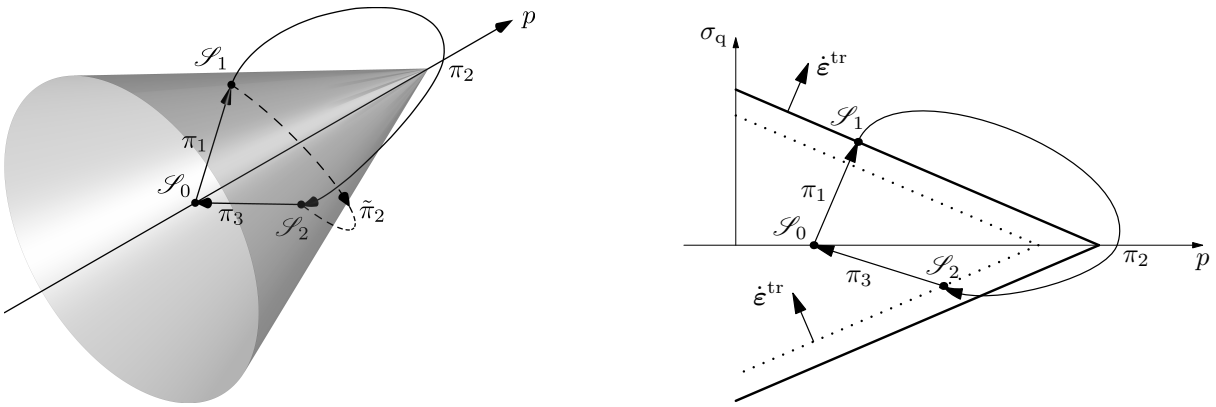

(a) Drucker-Prager limit surfaces. For illustration purposes the forward- and reverse-transformation limit surfaces are chosen to coincide $[Y_f(\xi) \equiv Y_r(\xi)]$.

(b) Cross-section of the limit surfaces for forward (solid) and reverse transformation (dotted) containing the hydrostatic axis and loading paths ($p - \sigma_{\mathrm{q}}$ plane).

Figure 1: Conical limit surfaces and loading paths in stress space.

while the transformation is not complete, by choosing a path tangential to the limit surface. This corresponds to neutral loading.

The total inelastic strain over a full loading-unloading cycle, i.e. the residual transformation strain after completion of the reverse transformation

$$\boldsymbol{\varepsilon}_{\mathrm{t}}^{\mathrm{tr}} \equiv \boldsymbol{\gamma}_{\mathrm{t}}^{\mathrm{tr}} - \frac{1}{3}\nu_{\mathrm{t}}^{\mathrm{tr}}\mathbf{1} = \oint \dot{\xi}\boldsymbol{N}\left(\boldsymbol{\sigma}\right)\mathrm{d}t = \sum_{i=1}^{3}\int_{\pi_i}\dot{\xi}\boldsymbol{N}\left(\boldsymbol{\sigma}\right)\mathrm{d}t \tag{8}$$

is expected to be smaller than the transformation strain after completion of the cd-Si $\rightarrow$ β-Si transformation, i.e.

$$\left\|\boldsymbol{\gamma}_{\mathrm{t}}^{\mathrm{tr}}\right\| \leqslant \left\|\boldsymbol{\gamma}^{\mathrm{tr}}\big|_{\mathscr{S}_1}\right\| , \tag{9a}$$

$$\nu_{\mathrm{t}}^{\mathrm{tr}} \leqslant \nu^{\mathrm{tr}}\big|_{\mathscr{S}_1} . \tag{9b}$$

In the case of proportional loading along π_1 the flow direction $\boldsymbol{N}\left(\boldsymbol{\sigma}\right) =: \boldsymbol{N}_f$ will remain unaltered throughout the loading process, i.e. $\dot{\boldsymbol{\varepsilon}}_{\pi_1}^{\mathrm{tr}} = \dot{\xi}\boldsymbol{N}_f$ and hence $\Delta\boldsymbol{\varepsilon}_{\pi_1}^{\mathrm{tr}} = \Delta\xi_f\boldsymbol{N}_f$. Similarly, $\Delta\boldsymbol{\varepsilon}_{\pi_3}^{\mathrm{tr}} = \Delta\xi_r\boldsymbol{N}_r$. On the intermediate loading path no inelastic deformation occurs, i.e. $\Delta\boldsymbol{\varepsilon}_{\pi_2}^{\mathrm{tr}} = 0$. Therefore, the total inelastic strain is computed to be $\boldsymbol{\varepsilon}_{\mathrm{t}}^{\mathrm{tr}} = \Delta\xi_f\boldsymbol{N}_f + \Delta\xi_r\boldsymbol{N}_r$.

A rather enlightening loading path is illustrated in Fig. 1. A sample is uniaxially loaded along π_1 until completion of the semiconductor to metal transformation at $\mathscr{S}_1$. Then, via π_2, the hydrostatic stress is increased beyond the intersection of the limit surface with the p-axis and deviatoric stress is applied; subsequently, the stress is relaxed onto the limit surface for reverse transformation at $\mathscr{S}_2$. Finally, the stress is returned to the initial state $\mathscr{S}_0$ via π_3, transforming the β-Si phase into a-Si. Hence, $\Delta\xi_f = -\Delta\xi_r =: \Delta\xi$, resulting in

$$\boldsymbol{\varepsilon}_{\mathrm{t}}^{\mathrm{tr}} = \Delta\xi\left(\boldsymbol{N}_f - \boldsymbol{N}_r\right) . \tag{10}$$

From Fig. 1(b) it is immediately clear that $\mathrm{tr}\left(\boldsymbol{N}_r\right) = \mathrm{tr}\left(\boldsymbol{N}_f\right)$, while $\boldsymbol{N}_r' = -\boldsymbol{N}_f'$. Therefore, Eq. (10) reduces to

$$\boldsymbol{\varepsilon}_{\mathrm{t}}^{\mathrm{tr}} = 2\Delta\xi\boldsymbol{N}_f' = 2\,\boldsymbol{\gamma}^{\mathrm{tr}}\big|_{\mathscr{S}_1} \tag{11}$$

$$\Rightarrow \left\|\boldsymbol{\gamma}_{\mathrm{t}}^{\mathrm{tr}}\right\| = 2\left\|\boldsymbol{\gamma}^{\mathrm{tr}}\big|_{\mathscr{S}_1}\right\| \tag{12}$$

i.e. after the reverse transformation the volumetric inelastic strain indeed vanishes, while the deviatoric inelastic strain doubles, which is in contradiction to (9a). This example is fairly general. For cylindrical limit surfaces the path $\tilde{\pi}_2$ would replace π_2 [see Fig. 1(a)], leaving the rest of the argumentation unchanged.

3.2 Discussion

The discovered discrepancy is caused by the model's failure to account for reorientation effects in the dense phase as well as to properly relate the direction of inelastic flow in unloading to the current transformation strain.

Similar problems occur in the constitutive modeling of the superelastic response of shape memory alloys (SMAs). In this community several approaches to this issue have been published [see e.g. Auricchio et al. (2007) or Panico and Brinson (2007)]. However, it should be noted that these efforts are mostly restricted to pressure independent, isochoric phase transitions, which is appropriate for SMAs, but not for materials such as silicon.

However, it is clear that for a purely volumetric reverse transformation the equal sign in (9a) holds. In this case $\boldsymbol{\varepsilon}_{\mathrm{t}}^{\mathrm{tr}}$ will be independent of the point on the limit surface $\mathscr{S}_2$ at which unloading takes place. Further, fixing the direction of inelastic flow reduces the number of parameters in the model, thus simplifying the identification procedure. This approach was used in the work of Budnitzki and Kuna (2012).

4 A Constitutive Model for Silicon

A detailed description of the proposed constitutive model has been published elsewhere (Budnitzki and Kuna, 2012). Hence, only a brief account of the constitutive equations is given here.

If, as a simplifying assumption, no distinction between the enthalpies of the different phases is made, the state function can be written as

$$\mathscr{E}(\boldsymbol{\sigma},\boldsymbol{\alpha}) = \mathscr{E}^{\mathrm{el}}(\boldsymbol{\sigma}) + \boldsymbol{\sigma} : \left(\boldsymbol{\gamma}^{\mathrm{tr}} - \frac{1}{3}\nu^{\mathrm{tr}}\mathbf{1}\right) + \mathscr{E}^{\mathrm{h}}\left(\nu^{\mathrm{tr}}\right) + \mathscr{I}_{\dot{\nu}^{\mathrm{tr}}}(\nu^{\mathrm{tr}})\,. \tag{13}$$

Here $\mathscr{E}^{\mathrm{el}}$ is the elastic portion of the GIBBS free enthalpy and $\mathscr{E}^{\mathrm{h}}$ is responsible for transformation hardening. The symbol $\mathscr{I}_{\dot{\nu}^{\mathrm{tr}}}(\nu^{\mathrm{tr}})$ denotes the indicator function of the interval $[0,\nu^{\mathrm{tr}}]$.

It is assumed that energy is dissipated during the motion of phase boundaries, i.e. when the phase content ξ or, as discussed above, the volumetric transformation strain ν^{tr} change. This can be written as

$$\mathscr{D}\left(\dot{\boldsymbol{\alpha}},\boldsymbol{\alpha}\right) = \mu\left(p,\nu^{\mathrm{tr}},s\right)\dot{\nu}^{\mathrm{tr}} \geqslant 0\,, \tag{14}$$

where $s := \mathrm{sign}\left(\dot{\nu}^{\mathrm{tr}}\right)$, i.e. $s=+1$ for forward and $s=-1$ for reverse transformation. To control the direction of inelastic flow, the dissipation function is supplemented with the kinematic constraint

$$\mathscr{C}(\boldsymbol{\sigma},\boldsymbol{\alpha},\dot{\boldsymbol{\alpha}}) := \dot{\nu}^{\mathrm{tr}} + \sqrt{\frac{2}{3}}\beta\left(p,\nu^{\mathrm{tr}},s\right)\|\dot{\boldsymbol{\gamma}}^{\mathrm{tr}}\| = 0\,. \tag{15}$$

It can be shown that the resulting limit functions in the space of thermodynamic forces are

$$\Phi_f\left(\boldsymbol{\sigma},\boldsymbol{\chi},\boldsymbol{\alpha}\right) = \chi_{\mathrm{q}} - \left|\beta\left(p,\nu^{\mathrm{tr}},+1\right)\right|\left[\mu\left(p,\nu^{\mathrm{tr}},+1\right) - \chi_{\mathrm{p}}\right] = 0\,, \tag{16a}$$

$$\Phi_r\left(\boldsymbol{\sigma},\boldsymbol{\chi},\boldsymbol{\alpha}\right) = \left|\beta\left(p,\nu^{\mathrm{tr}},-1\right)\right|\left[\mu\left(p,\nu^{\mathrm{tr}},-1\right) - \chi_{\mathrm{p}}\right] - \chi_{\mathrm{q}} = 0\,. \tag{16b}$$

The limit functions in principle stress space are obtained from (16) using Equations (3) and (13)

$$\begin{aligned} F_f\left(\boldsymbol{\sigma},\boldsymbol{\alpha}\right) &= \sigma_q - \left|\beta\left(p,\nu^{\mathrm{tr}},+1\right)\right|\left\{\mu\left(p,\nu^{\mathrm{tr}},+1\right) - \left[p - p_{\mathrm{Y}}\left(\nu^{\mathrm{tr}}\right)\right]\right\} \\ &=: \sigma_q - \tilde{\mu}\left(p,\nu^{\mathrm{tr}},+1\right)\,, \end{aligned} \tag{17a}$$

$$\begin{aligned} F_r\left(\boldsymbol{\sigma},\boldsymbol{\alpha}\right) &= \left|\beta\left(p,\nu^{\mathrm{tr}},-1\right)\right|\left\{\mu\left(p,\nu^{\mathrm{tr}},-1\right) - \left[p - p_{\mathrm{Y}}\left(\nu^{\mathrm{tr}}\right)\right]\right\} - \sigma_q \\ &=: \tilde{\mu}\left(p,\nu^{\mathrm{tr}},-1\right) - \sigma_q\,, \end{aligned} \tag{17b}$$

where $p_{\mathrm{Y}}\left(\nu^{\mathrm{tr}}\right) := -\frac{\partial\mathscr{E}^{\mathrm{h}}\left(\nu^{\mathrm{tr}}\right)}{\partial\nu^{\mathrm{tr}}}$. The direction of inelastic flow is determined from (2) resulting in

$$\dot{\boldsymbol{\gamma}}^{\mathrm{tr}} = \dot{\lambda}\frac{\partial\Phi_{(\cdot)}\left(\boldsymbol{\sigma},\boldsymbol{\chi},\boldsymbol{\alpha}\right)}{\partial\boldsymbol{\chi}'} = \dot{\tilde{\lambda}}\sqrt{\frac{3}{2}}\frac{\boldsymbol{\chi}'}{\|\boldsymbol{\chi}'\|}\,, \tag{18a}$$

$$\dot{\nu}^{\mathrm{tr}} = \dot{\lambda}\frac{\partial\Phi_{(\cdot)}\left(\boldsymbol{\sigma},\boldsymbol{\chi},\boldsymbol{\alpha}\right)}{\partial\chi_{\mathrm{p}}} = \dot{\tilde{\lambda}}\left|\beta\left(p,\nu^{\mathrm{tr}},s\right)\right|\,, \tag{18b}$$

where $\dot{\tilde{\lambda}}$ is a rescaled consistency parameter with $\mathrm{sign}\left(\dot{\tilde{\lambda}}\right) = \mathrm{sign}\left(\dot{\nu}^{\mathrm{tr}}\right)$. The description of the constitutive behaviour is completed by specifying the functions $\tilde{\mu}\left(p,\nu^{\mathrm{tr}},s\right)$ and $\beta\left(p,\nu^{\mathrm{tr}},s\right)$.

5 Choice of Functional Forms for the Limit Surfaces

Experimental results suggest to choose hyperboloids of revolution aligned along the hydrostatic axis and closed in compression as limit surfaces [see (Budnitzki and Kuna, 2012) for further discussion]. For this case Sec. 3.2 implies that the direction of inelastic flow during cd-Si → β-Si transformation can be used as a fitting parameter to match experimental results, whereas the β-Si → a-Si transformation should be kept purely volumetric to prevent undesired model behavior in non-proportional loading.

Considering the expressions for the limit functions given by Eqs. (17), an appropriate choice for $\tilde{\mu}$ is

$$\tilde{\mu}\left(p,\nu^{\mathrm{tr}},s\right) := \frac{b}{a}\sqrt{\left(\left[p - p_{\mathrm{Y}}\left(\nu^{\mathrm{tr}}\right) - H(-s)d\right] - a\right)^2 - a^2}\,, \tag{19}$$

where H is the unit-step function and a, b and d are shape parameters. The resulting surface for forward transfor-

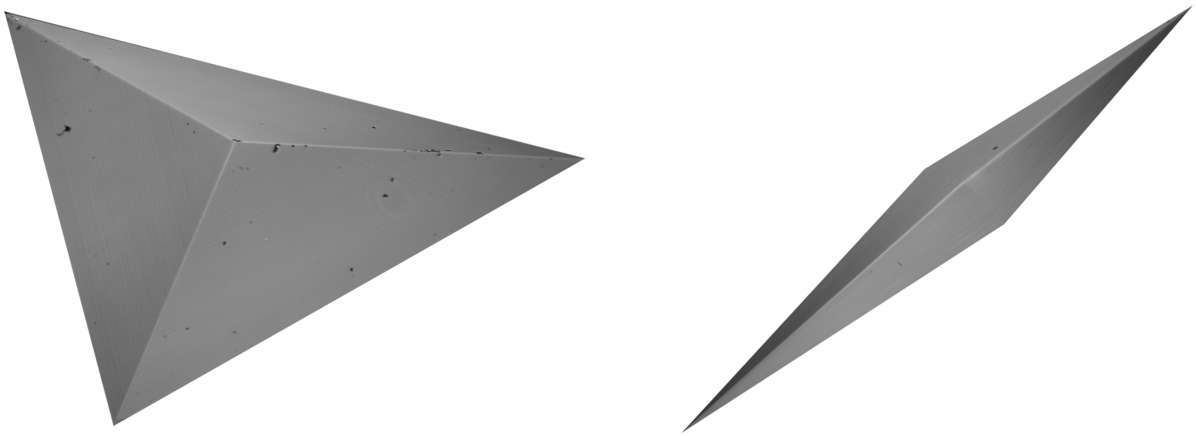

(a) BERKOVICH indenter tip. (b) KNOOP indenter tip.

Figure 2: Micrographs of indenter tips obtained using laser confocal microscopy.

mation intersects the hydrostatic axis at $p = p_{\mathrm{Y}}\left(\nu^{\mathrm{tr}}\right) := p_{\mathrm{Y0}} + h\nu^{\mathrm{tr}}$. For this case $\beta\left(p, \nu^{\mathrm{tr}}, s\right)$ is chosen as

$$\beta\left(p, \nu^{\mathrm{tr}}, +1\right) := \frac{b'}{a} \frac{p - p_{\mathrm{Y}}\left(\nu^{\mathrm{tr}}\right) - a}{\sqrt{\left(\left[p - p_{\mathrm{Y}}\left(\nu^{\mathrm{tr}}\right)\right] - a\right)^2 - a^2}}\,, \tag{20}$$

which, depending on the choice of b', results in associated $(b' = b)$ or non-associated flow. It can be easily shown that dissipation is non-negative throughout the loading process if $\frac{b}{b'} \geq 1$.

During reverse transformation, the constraint $\mathscr{C}_r(\boldsymbol{\sigma}, \boldsymbol{\alpha}, \dot{\boldsymbol{\alpha}}) := \|\dot{\boldsymbol{\gamma}}^{\mathrm{tr}}\| = 0$ is assumed. This condition can be obtained from (15) in the limit $\beta\left(p, \nu^{\mathrm{tr}}, -1\right) \to \infty$, or, using definition (20), $b' \to \infty$. It can be seen from Eqs. (17) and (19), that the shape of the limit surface in principal stress space remains unaffected, as the hyperboloid is only shifted by d along the hydrostatic axis.

6 Experimental Procedures

The experimental force-displacement curves have been obtained using the UNAT (Asmec GmbH) nanoindenter with BERKOVICH and KNOOP indenter tips, respectively. High resolution optical micrographs of the indenter tips (see Fig. 2) have been acquired using the confocal laser scanning microscopy (CLSM) technique. Imaging has been performed with Olympus Lext OLS4000 microscope. The obtained surface profiles have been used to verify the face angles of both indenter tips. In addition, the area function of the BERKOVICH indenter was independently determined using two reference materials.

The experimental curves shown in Figs. 3 and 5(b) have been obtained from indentations in a (100) single crystal silicon wafer and represent an average of 10 force-displacement curves respectively. The load was applied at a rate of 2 mN/s.

7 Numerical Results and Discussion

The numerical implementation of the novel constitutive model as a user material subroutine (UMAT) in the commercial finite element (FE) code ABAQUS/Standard as well as its response for homogeneous loading conditions have been presented in a previous work (Budnitzki and Kuna, 2012). The constitutive behavior is fully determined by 8 parameters: The YOUNG's modulus Y, the POISSON's ratio ν, the transformation initiation pressure under hydrostatic loading p_{Y0}, the corresponding linear hardening modulus h, the constants a, b, b' that determine the shape of the limit surfaces and flow potential as well as the parameter d that prescribes the onset of reverse transformation in unloading. The POISSON's ratio, the transformation initiation pressure as well as the hardening modulus could be established from literature data, while E, b, b', and d were determined by fitting an axisymmetric model with a rigid sphero-conical indenter tip to experimentally obtained force displacement $(F - U)$ curves from nanoindentation with BERKOVICH indenter (Budnitzki and Kuna, 2012). The values are summarized in Tab. 1.

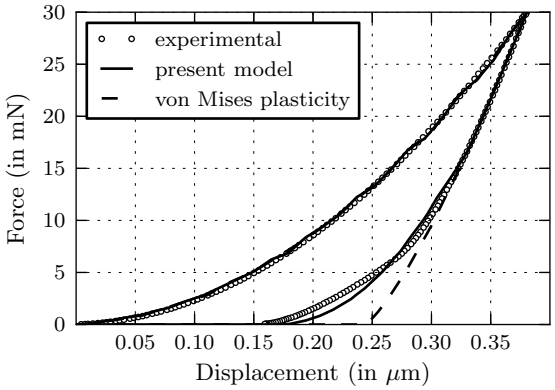

Figure 3: Experimental and simulated $F - U$ curves.

model parameter	value
E	136.59 GPa
ν	0.23
p_{Y0}	11.30 GPa
h	3.92 GPa
a	0.50 GPa
$\frac{b}{a}$	1.04
$\frac{b'}{a}$	0.99
d	4.80 GPa

Table 1: Model parameters.

The resulting fit of the experimental curve can be seen in Fig. 3. A curve obtained using ideal VON MISES plasticity (with elastic constants $E = 133.25$ GPa, $\nu = 0.23$ and yield stress $\sigma_{\mathrm{Y}} = 5.64$ GPa) is shown for comparison in order to highlight the importance of reverse phase transformation for the correct simulation of indentation in silicon.

To assess the quality and - to a certain degree - the uniqueness of the obtained description it is helpful to consider the effect of the individual parameters on the shape of the simulated $F - U$ curve. The YOUNG's modulus (or, to be more specific, the so called reduced modulus E_r) can be obtained independently of the inelastic properties in accordance with the Oliver and Pharr (1992) procedure by evaluating the slope of the $F - U$ curve at the point of load reversal. Hence, its effect can be clearly separated.

The effects of the parameters b and b', which characterize the shape of the limit surface for phase transition and the flow potential respectively, are illustrated in Figs. 4(a) and 4(b). An increase of b increases the maximal force at prescribed displacement $\hat{\delta}$, while simultaneously decreasing the residual depth of the indent. Changes in b' affect the residual depth, while leaving the maximum force almost at a constant value. Thus the main features of the force displacement curve can be adjusted independently. The parameter d determines the point at which the unloading curve begins to deviate from the elastic one. This allows for additional minor corrections of the residual depth after full unloading.

The above considerations show that indentation experiments with sharp indenter are particularly well suited to determine material parameters for the discussed constitutive model. As a result of this separation of effects, it can be expected that the obtained set of model parameters is specific to the material only and independent of the particular load case it was fitted to. To support this statement the numerical simulation of a KNOOP indentation experiment with parameters obtained from BERKOVICH indentation was performed. The KNOOP indenter is a very blunt, 4-sided pyramid with a rhombic base [see Fig. 2(b)] that leads to a stress state in the material, which differs

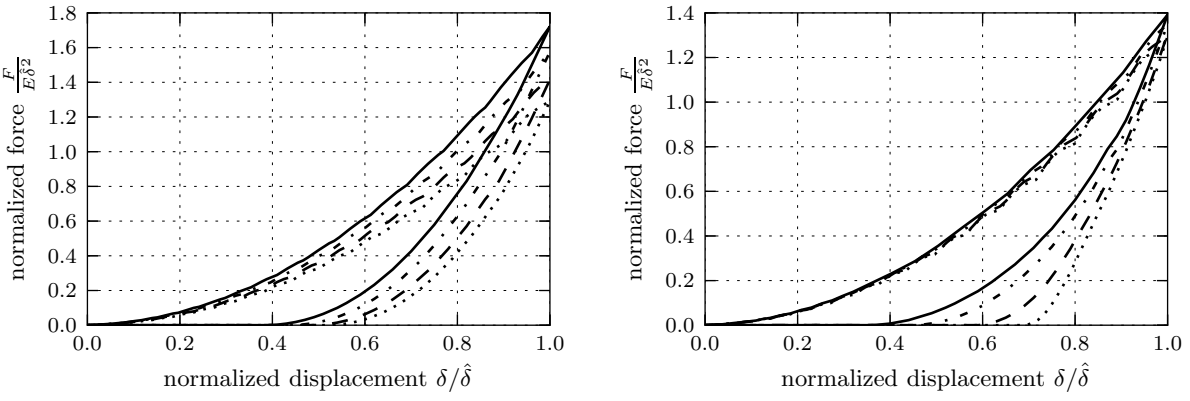

(a) Variation of b.

(b) Variation of b'.

Figure 4: Effect of the parameters b and b' on the simulated force displacement ($F - U$) curves for BERKOVICH indentation.

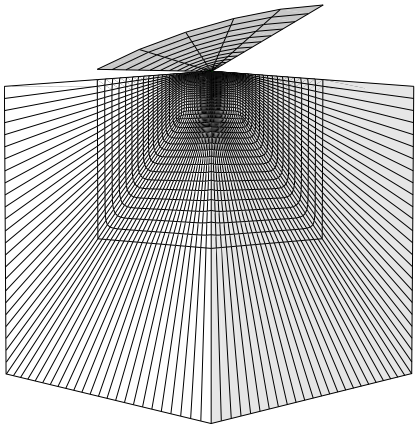

(a) FE mesh for KNOOP indentation simulations.

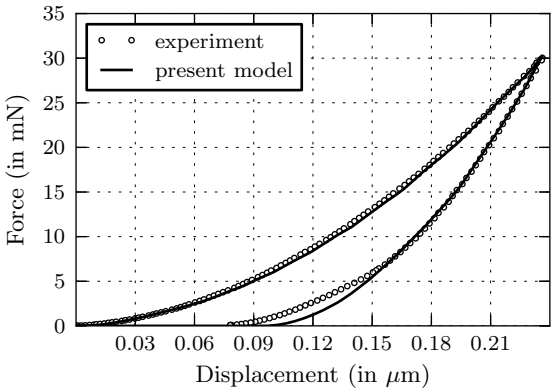

(b) Experimental and simulated KNOOP indentation curves.

Figure 5: Simulated of KNOOP indentation experiments.

strongly from the one caused by the 3-sided BERKOVICH pyramid. Therefore, it can be considered appropriate for verification purposes.

Due to the elongated shape of the KNOOP indenter tip an axisymmetric model is inappropriate. Therefore, a quarter 3D FE-model was used [see Fig. 5(a)]. A sufficiently large region of the silicon sample was meshed with hexahedral elements C3D8 and embedded into an elastic half-space implemented with infinite elements CIN3D8. Displacements were fixed at the infinite boundary. The indenter was modeled with rigid elements R3D3 and R3D4. The obtained force displacement curve is shown in Fig. 5(b) along with the experimental reference curve. A very reasonable match is obtained, which verifies the predictive capability of the constitutive model.

8 Summary and Conclusion

It has been discussed that for modeling (partially) reversible, stress induced phase transformations the direction of inelastic flow - especially during reverse phase transformation - cannot be chosen arbitrarily. This is important in order to prevent erratic model behavior in non-proportional loading. However, it has been demonstrated that no problems occur if the inelastic flow during reverse transformation is purely volumetric.

Further, it has been shown that indentation experiments with sharp indenter are particularly suited for determining model parameters for the constitutive model of Budnitzki and Kuna (2012). This was verified by the successful numerical simulation of an independent experiment that the model was not explicitly fitted to.

Acknowledgements: The authors acknowledge Thomas Behm for his assistance with the CLSM imaging. This work was performed within the Cluster of Excellence "Structure Design of Novel High-Performance Materials via Atomic Design and Defect Engineering (ADDE)" that is financially supported by the European Union (European regional development fund) and by the Ministry of Science and Art of Saxony (SMWK).

References

Auricchio, F.; Reali, A.; Stefanelli, U.: A three-dimensional model describing stress-induced solid phase transformation with permanent inelasticity. *Int. J. Plasticity*, 23, 2, (2007), 207–226.

Bhagavat, S.; Kao, I.: Ultra-low load multiple indentation response of materials: In purview of wiresaw slicing and other free abrasive machining (fam) processes. *Int. J. Mach. Tool. Manu.*, 47, 3-4, (2007), 666–672.

Budnitzki, M.; Kuna, M.: A thermomechanical constitutive model for phase transformations in silicon under pressure and contact loading conditions. *Int. J. Solids Struct.* (2012).

Cook, R.: Strength and sharp contact fracture of silicon. *J. Mater. Sci. (USA)*, 41, 3, (2006), 841 – 872.

Domnich, V.; Gogotsi, Y.: Phase transformations in silicon under contact loading. *Rev. Adv. Mater. Sci.*, 3, (2002), 1–36.

Gerk, A.; Tabor, D.: Indentation hardness and semiconductor-metal transition of germanium and silicon. *Nature*, 271, 5647, (1978), 732–733.

Han, W.; Reddy, B.: *Plasticity: mathematical theory and numerical analysis*. Springer (1999).

Hu, J.; Merkle, L.; Menoni, C.; Spain, I.: Crystal data for high-pressure phases of silicon. *Phys. Rev. B*, 34, 7, (1986), 4679–4684.

Kiriyama, T.; Harada, H.; Yan, J.: Finite element modeling of high-pressure deformation and phase transformation of silicon beneath a sharp indenter. *Semicond. Sci. Tech.*, 24, (2009), 025014.

Lawn, B.: *Fracture of brittle solids*. Cambridge Univ Press (1993).

Mcmahon, M.; Nelmes, R.: New high-pressure phase of Si. *Phys. Rev. B*, 47, 13, (1993), 8337–8340.

Mcmahon, M.; Nelmes, R.; Wright, N.; Allan, D.: Pressure-dependence of the Imma phase of silicon. *Phys. Rev. B*, 50, 2, (1994), 739–743.

Oliver, W.; Pharr, G.: An improved technique for determining hardness and elastic-modulus using load and displacement sensing indentation experiments. *Journal of Materials Research*, 7, 6, (1992), 1564–1583.

Panico, M.; Brinson, L.: A three-dimensional phenomenological model for martensite reorientation in shape memory alloys. *Journal of the Mechanics and Physics of Solids*, 55, 11, (2007), 2491–2511.

Vodenitcharova, T.; Zhang, L.: A mechanics prediction of the behaviour of mono-crystalline silicon under nano-indentation. *Int. J. Solids Struct.*, 40, 12, (2003), 2989–2998.

Vodenitcharova, T.; Zhang, L.: A new constitutive model for the phase transformations in mono-crystalline silicon. *Int. J. Solids Struct.*, 41, 18-19, (2004), 5411–5424.

Wang, T. H.; Fang, T.-H.; Lin, Y.-C.: A numerical study of factors affecting the characterization of nanoindentation on silicon. *Mat. Sci. Eng. A-Struct.*, 447, 1-2, (2007), 244 – 253.

Yoshino, M.; Aoki, T.; Chandrasekaran, N.; Shirakashi, T.; Komanduri, R.: Finite element simulation of plane strain plastic-elastic indentation on single-crystal silicon. *Int. J. Mech. Sci.*, 43, 2, (2001), 313–333.

Zhang, L.; Mahdi, M.: The plastic behaviour of silicon subjected to micro-indentation. *J. Mater. Sci.*, 31, 21, (1996), 5671–5676.

Ziegler, H.: *Introduction to Thermomechanics*. Amsterdam: North-Holland Publishing Company (1983).

Ziegler, H.; Wehrli, C.: The derivation of constitutive relations from the free energy and dissipation function. *Adv. Appl. Mech.*, 25, (1987), 183–238.

Address: TU Bergakademie Freiberg, Institute of Mechanics and Fluid Dynamics, Lampadiusstr. 4, 09599 Freiberg
Author to whom all correspondence should be addressed: michael.budnitzki@imfd.tu-freiberg.de